

One-dimensional Excitations in Superfluid ^4He and ^3He - ^4He Mixture Films Adsorbed in Porous Materials

Hyung Cho* and Gary A. Williams

Department of Physics and Astronomy, University of California, Los Angeles, CA 90095

(Dated: October 31, 2018)

A normal-fluid component varying as T^2 is observed at very low temperatures in superfluid ^4He and ^3He - ^4He mixture films adsorbed in alumina powder. The normal fluid appears to arise from thermally excited third sound that has one-dimensional propagation characteristics. A Landau model of third sound excitations in an infinite cylindrical pore by Saam and Cole provides good agreement with the experimental measurements over a wide range of ^4He and ^3He coverages. However, it is unclear why the powder substrate can be modeled as having cylindrical pores.

PACS numbers: 67.70.+n, 67.40.Db, 67.40.Rp, 67.60.Fp

I. INTRODUCTION

The Landau theory of superfluid ^4He has been very successful in explaining the observed normal fluid density of the liquid in terms of the thermal excitations, the phonons and rotons.^{1,2} At low temperatures only phonons are thermally excited, and a well-known result of the Landau theory is that the normal fluid density ρ_n should then vary with temperature as²

$$\rho_n = \frac{2\pi^2}{45} \left(\frac{k_B^4}{\hbar^3 c_1^5} \right) T^4. \quad (1)$$

Here c_1 the velocity of first sound. Experimental measurements at low temperatures are consistent with this expression for the normal fluid density^{3,4}, and an analogous T^3 dependence of the specific heat from the excited phonons is measured.⁵

For two-dimensional (2D) helium films on a flat substrate, the comparable excitations are propagating thickness oscillations, known as third sound.⁶ Density-functional theories⁷ of thin films show that these excitations are well-defined and have linear dispersion even for typical thermal wavelengths of order tens of Å. Applying the Landau model to this case gives an areal normal fluid density

$$\sigma_n = \frac{2\pi^2}{34.4} \left(\frac{k_B^3}{\hbar^2 c_3^4} \right) T^3 \quad (2)$$

where c_3 is the third-sound velocity. This T^3 variation has been observed in measurements on helium films adsorbed on flat substrates.^{8,9}

However, measurements of the normal-fluid density of helium films adsorbed in fine porous materials do not show the expected 2D behavior as above. This was observed in earlier measurements of films adsorbed in porous Vycor glass¹⁰ and in porous silica,¹¹ and is also seen in our measurements using an alumina powder substrate.^{12,13,14,15} For these substrates the normal-fluid density is found to vary as T^2 , indicative of a one-dimensional (1D) thermal excitation. Computing the

Landau theory for a 1D thickness oscillation yields for the normal-fluid density per unit length λ_n ,

$$\lambda_n = \frac{\pi}{3} \left(\frac{k_B^2}{\hbar c_3^3} \right) T^2. \quad (3)$$

This is also the limiting result found by Saam and Cole¹⁶ for third sound excitations in an infinitely long cylindrical pore. For a small pore diameter and very low temperatures the only modes excited are those propagating along the cylinder axis, since the modes transverse to the axis can only have wavelengths smaller than the pore diameter, and consequently high frequencies that make them energetically unfavorable at low T .

Since the torsion oscillator technique used in our experiments actually measures the superfluid mass per unit area, it is necessary to relate the linear and areal densities by assuming that the propagation is along a cylindrical pore of average diameter D_p , for which $\lambda_n = \sigma_n \pi D_p$. The normalized areal superfluid density is then

$$\frac{\sigma_s(T)}{\sigma_s(0)} = 1 - \frac{\sigma_n(T)}{\sigma_s(0)} = 1 - \beta' T^2 \quad (4)$$

where the coefficient of the T^2 term is

$$\beta' = \frac{k_B^2}{3 \hbar D_p c_3^3 \sigma_s(0)}. \quad (5)$$

In this paper we show that the Landau model for 1D excitations provides good agreement with our low-temperature measurements of the normal-fluid density in ^4He and ^3He - ^4He mixture films adsorbed on a porous substrate.

II. EXPERIMENT

The substrate used in our measurements is an Al_2O_3 powder of nominal diameter 500 Å. A slip-casting technique¹⁷ uses the surface tension force of water draining out of the powder to tightly pack the smaller powder grains into the voids

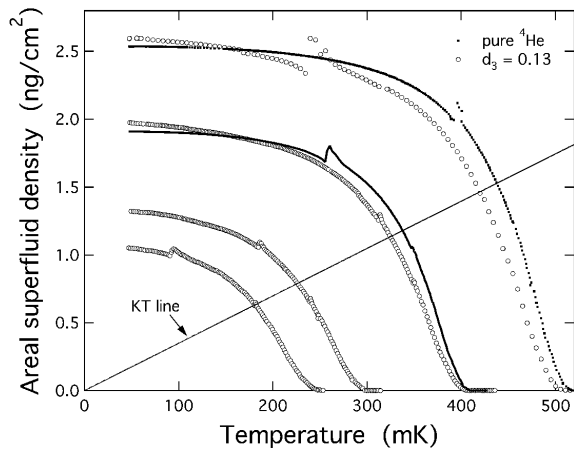


FIG. 1: Areal superfluid density versus temperature for two pure ^4He films (solid dots) with $d_4 = 0.50$ and 0.38 layers (upper and lower curves), and four ^3He - ^4He mixture films (open circles) with $d_3 = 0.13$ layers and (top to bottom) $d_4 = 0.61, 0.49, 0.37,$ and 0.31 layers

around larger grains. This leads to a relatively low sample porosity (ratio of the open volume to the total volume) of $P = 0.59$. A standard estimate¹⁸ of the pore size of our samples based on the porosity yields 105 \AA . The volume of the sample is 5.07 cm^3 , and its surface area is 146 m^2 .

The helium samples are condensed into the cell from measured amounts of gas at room temperature, while the cell is maintained below 0.5 K with a dilution refrigerator. The filling capillary of inside diameter 0.25 mm is 1 m long and is not thermally anchored except at 4.2 K and the sample chamber. After condensing ^3He the sample is warmed to 4.2 K for 24 hours to anneal the sample and assure uniform coverage of the ^3He .¹⁹ This step is not necessary when adding further superfluid ^4He . To characterize the helium coverages we take one layer of ^4He to be $12.8 \text{ } \mu\text{moles/m}^2$ and one layer of ^3He as $10.7 \text{ } \mu\text{moles/m}^2$, corresponding to the bulk liquid densities at low pressure. For the first few layers of the film this will be an overestimate of the actual number of atomic layers, since these are closer to the solid density due to the attractive substrate potential, but it should be a reasonable approximation for the top layer or two farthest from the substrate. We find that the first 2.7 layers of ^4He are not superfluid at any temperature, forming the inert "dead" layers known from earlier investigations.⁶ We define a ^4He thickness d_4 as the thickness in excess of the dead layer; d_4 is then the thickness of the superfluid portion of the film at $T = 0$, with no ^3He added. A torsion oscillator is employed to determine the superfluid mass of the film, as described in Refs. 12 and 15. By measuring the extrapolated $T = 0$ period shift of the oscillator as a function of the mass of the helium added the areal superfluid density of the films can be calibrated.

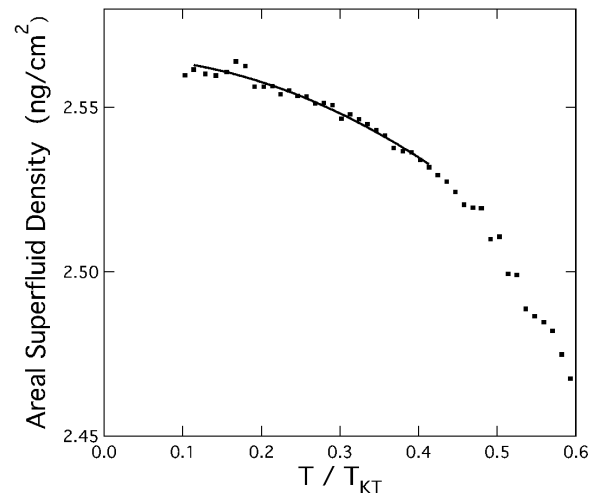


FIG. 2: Areal superfluid density at low temperatures for a film of pure ^4He (from Ref. 15) with a superfluid thickness of 0.55 layers and $T_{KT} = 453 \text{ mK}$. The solid line is the fit to Eq. (4).

III. RESULTS

An example of our data for the areal superfluid density of both pure ^4He and ^3He - ^4He mixture films is shown in Fig. 1. Further data can be found in References 12,13,14,15. As shown by the correspondence with the critical Kosterlitz-Thouless (KT) universal line in this data, the superfluid transition of the films is mediated by thermally excited vortex excitations. There is no sharp drop of the superfluid density to zero at the temperature T_{KT} where the data crosses the KT line because of the finite pore size of the substrate,²⁰ which acts to broaden the transition region. The small glitches in the data of Fig. 1 are due to the third-sound modes of our cylindrical cell, which couple weakly to the torsional mode. The glitches mark the mode-crossing points where the the third-sound frequencies match the torsional frequency as the superfluid density decreases with temperature.

Of interest in the present paper is the low-temperature regime of the data, $T \leq 0.5 T_{KT}$, where the density of thermally excited KT vortex pairs is negligible. In this regime the data can be accurately fit to the form of Eq. (4), and values of β' can be extracted. Figure 2 shows the low-temperature region for one data set of pure ^4He from Ref. 15, where the solid line shows the two-parameter fit with values of $\beta' = 0.36 \text{ K}^{-1}$ and $\sigma_s(0) = 2.565 \text{ ng/cm}^2$. More general fits including terms linear and cubic in T were tried, but the fit coefficients for such terms were negligibly small. Figure 3 shows the values of β' obtained for a series of pure ^4He films¹² of different thickness, plotted versus d_4 . Also plotted in Fig. 3 are the unpublished results of McQueeney²¹ for a similar set of films in porous Vycor glass. Both show a fairly rapid increase in β' as d_4 (and T_c) is reduced, with the Vycor data being about a factor of two larger than the alumina powder results. The higher values found in the Vycor sample are roughly consistent with Eq. (5), which predicts that β' should scale as the inverse of

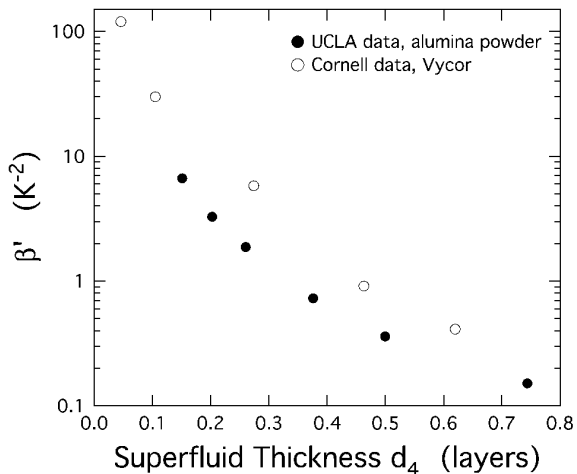


FIG. 3: The coefficient β' of the T^2 term as a function of the superfluid thickness for pure ^4He films. The open circles are the porous Vycor glass data of Ref. 21.

the average pore diameter: the pore diameter of the Vycor is thought to be about 75 \AA , while as noted above the average pore diameter of our slip-cast sample is of order 100 \AA . The scaling with the inverse pore size also accounts for the considerably larger values of β' seen with porous silica substrates¹¹ having 25 \AA pores, causing the T^2 term to dominate the superfluid density over nearly the entire temperature range up to the superfluid transition temperature.

In Fig. 4 our β' data is plotted for ^3He - ^4He mixture films, where the ^3He thickness d_3 is held constant and d_4 is varied by adding further ^4He . The values of β' are considerably increased with the addition of ^3He , something which is readily evident comparing the mixture film curves in Fig. 1 with the curves for pure ^4He at the lowest temperatures. The error bars reflect the increasing uncertainties in the fits as T_c is reduced with increasing ^3He coverage, which puts an increasingly smaller fraction of the data at temperatures below $0.5 T_{KT}$. The largest error bar in Fig. 4, for the film with $d_4 = 0.55$ and $d_3 = 0.73$, comes from the fits to the lowest curve in Fig. 1 of Ref. 15. With $T_{KT} = 139 \text{ mK}$ for this data only a few points are available in the low-temperature regime for making a rough estimate of β' .

The fits to the data also give the $T = 0$ value of the areal superfluid density, shown in Fig. 5 as a function of d_4 . As expected the variation is linear in the ^4He coverage, but the addition of ^3He suppresses some fraction of the superfluid density. Curves very similar to this have been observed for mixture films on flat Mylar substrates²².

To compare the data of Fig. 4 with the Landau model of Eq. (5), it is necessary to measure the third-sound velocity. This can also be obtained from the torsion-oscillator data, due to the third-sound glitches noted above. These third-sound resonances are even more visible as dissipation peaks in the inverse Q factor of the oscillator, measured by monitoring the drive voltage needed to keep the amplitude of the oscillator a

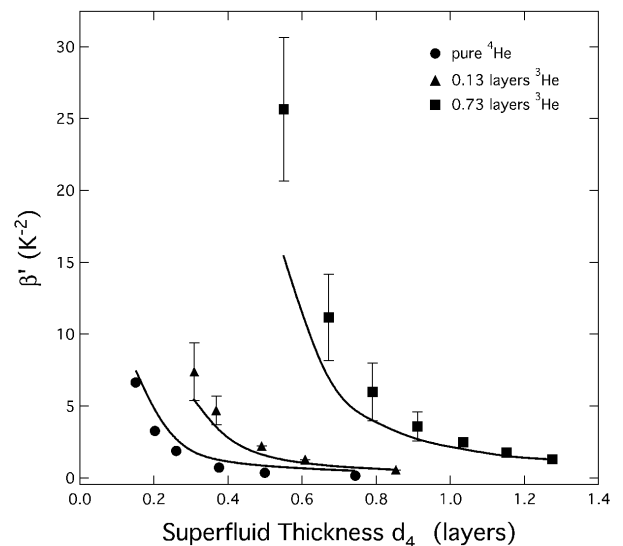


FIG. 4: β' for ^3He - ^4He mixture films as a function of the ^4He superfluid coverage. The solid curves are the Landau theory of Eq. (5).

constant. Examples of this data are shown in Fig. 3 of Ref. 12. For the cylindrical sample geometry with radius R and length L_z , and taking the boundary condition that there be no heat flow from the outer surfaces of the powder sample, the resonant frequencies of the third sound are given by

$$\omega_{m n n_z} = \frac{c_3}{2} \sqrt{\left(\frac{\alpha'_{mn}}{\pi R}\right)^2 + \left(\frac{n_z}{L_z}\right)^2} \quad (6)$$

where α'_{mn} is the n_{th} zero of the derivative of the Bessel function J_m . The geometrical factors are known, and hence the third sound velocity can be determined from the oscillator frequency. Since the resonances are determined by the mode-crossing condition they occur at different temperatures for each mode, and in order to compare them the velocities are multiplied by the factor $\sqrt{\sigma_s(0)/\sigma_s(T)}$, to extrapolate to the $T = 0$ value. It is found that the lowest five modes of a given film yield the same low-temperature speed to within about 5%, and the average value is taken. The third sound speed c_3 is that for the film in the porous medium, and is smaller than that for the same film on a flat substrate by the index of refraction that accounts for the tortuosity of the multiply-connected film on the powder grains.²³ This can be deduced from the change in slope of the oscillator's period shift versus added helium when the film becomes superfluid; for the present slip-cast sample the index of refraction was 1.67.

Figure 6 shows the extrapolated third sound speeds at $T = 0$ versus superfluid film thickness for the pure ^4He films and for two mixture film sets. The variation with superfluid thickness is just that expected for these very thin films where the Van der Waals restoring force dominates: a variation as $\sqrt{d_4}$ at small d_4 , and then a turnover towards a maximum at larger thickness as the restoring force diminishes with increasing total film thickness. The addition of ^3He lowers the third

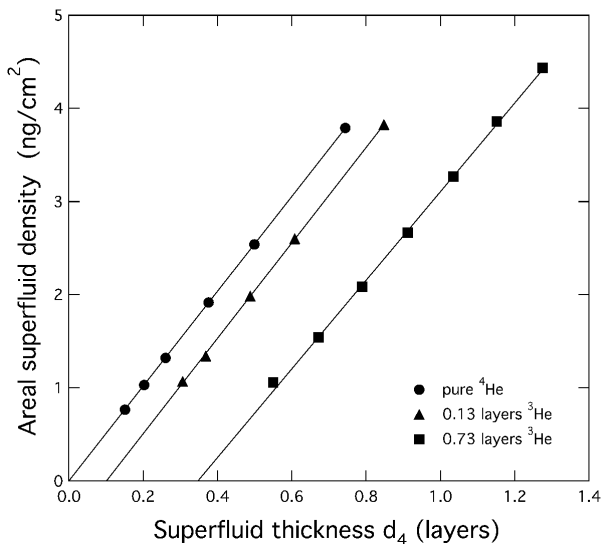


FIG. 5: Zero-temperature superfluid areal density as found from the fits of the data to Eq. (4).

sound velocity since the superfluid density is decreased,²⁴ as in Fig. 5.

From the data shown in Figs. 5 and 6 the predicted coefficient β^l of Eq. (5) can be evaluated for each of the film thicknesses shown in Fig. 4; the solid lines in the figure are spline fits to the resulting values. D_p in Eq. (5) was adjusted to get the best match to the data, and the resulting value of 48 \AA is at least roughly consistent with our estimated pore size of 100 \AA . As can be seen in Fig. 4 the agreement with the Landau expression for 1D excitations is quite good for the entire range of ^4He and ^3He coverages, considering that only the single parameter D_p was adjusted to get the agreement.

IV. DISCUSSION

Although the Landau theory provides a good description of the experimental results, the reasons why the excitations display one-dimensional behavior in the geometry of the slip-cast powder remain unclear. In the theory of Saam and Cole¹⁶ the cylindrical geometry with pore length much greater than the diameter is crucial to the appearance of 1D behavior at low temperatures. There is no obvious reason why the pores in the powder can be modeled in this fashion. The frequency of third sound with energy $k_B T$ at a temperature of 0.3K is $k_B T / 2\pi\hbar = 1 \times 10^{10} \text{ Hz}$, corresponding to a wavelength of order 20 \AA . This is smaller than the pore diameter, and one might expect instead 2D propagation characteristics for that case, as seen on the flat substrates. An unknown factor is the mean free path of the high-frequency third sound, which could well be less than the pore size.

One consideration which might be important is the orientation of the pores with respect to the direction of the superflow imposed by the torsional motion. Quasi-cylindrical pores

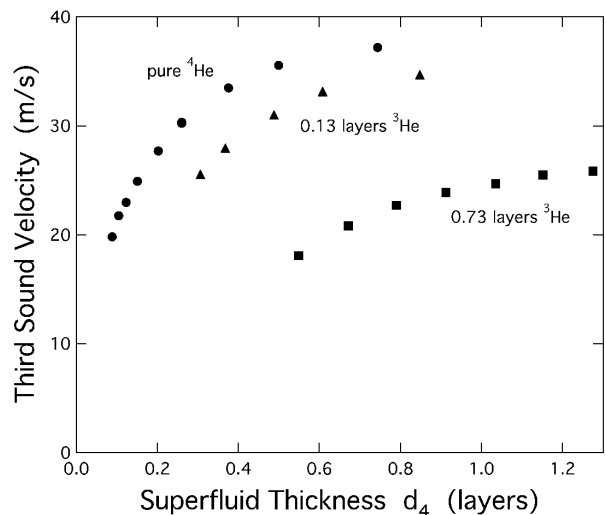


FIG. 6: Third sound velocities extrapolated to $T = 0$.

whose axis is parallel to the motion contribute considerably more to the measured superfluid fraction than those perpendicular to the motion; this is the origin of the index of refraction for the porous materials. If the third-sound scattering process which transfers momentum to the substrate is also anisotropic in the cylindrical channel, such that only propagation directions along the axis contribute, this could give possibly lead to a 1D behavior of the superfluid density.

A further possibility is that the points where the grains make contact with each other may play a role. All of the flow between the grains is channeled into these regions, which are probably smaller in extent than the $\approx 20 \text{ \AA}$ thermal third-sound wavelength. They would effectively be 1D channels, and since the flow velocity is locally much higher than the average, these regions might account for a disproportionate share of the reduction of the superfluid density. It is clear that further theoretical work modeling superflow and third-sound propagation in a porous multiply-connected geometry will be needed to understand the observed effects.

An additional experimental signature of 1D propagation would be a low-temperature heat capacity linear in T . The Landau model yields for N cylindrical pores of length L a heat capacity

$$C = NL \left(\frac{\pi k_B^2}{6\hbar c_3} \right) T, \quad (7)$$

which is also the low-temperature limit of the calculation of Saam and Cole. However, experiments on superfluid films in Vycor over the thin-film range of coverages discussed here show heat capacities varying more as T^2 . The heat capacity is a more complicated quantity which also has considerable contributions from the "dead" layers, and this may be obscuring the contribution from the 1D third sound excitations.

ACKNOWLEDGMENTS

This work was supported by the National Science Foundation, Division of Materials Research, under grants DMR 95-00653 and DMR 97-31523.

REFERENCES

- * Present address: Jet Propulsion Laboratory, 4800 Oak Grove Blvd., Pasadena, CA 91109.
- ¹ D. Tilley and J. Tilley *Superfluidity and Superconductivity*, (A. Hilger, Bristol, 1990).
 - ² I. M. Khalatnikov, *An Introduction to the Theory of Superfluidity*, (Benjamin, New York, 1965).
 - ³ G. A. Williams and R. Rosenbaum, *Phys. Rev. B* **20**, 4738 (1979).
 - ⁴ Han-Ching Chu and one of the present authors (G. A. W.) have carried out further measurements on the same alumina sample discussed in this paper, but where the pores were completely filled with ⁴He. Fitting to the decreasing superfluid fraction between 100 and 600 mK for this case yields a power-law exponent with temperature of 3.7 ± 0.2 , consistent with the value of 4 expected for 3D behavior.
 - ⁵ N. Phillips, C. Waterfield, and J. Hoffer, *Phys. Rev. Lett.* **25**, 1260 (1970).
 - ⁶ K. R. Atkins and I. Rudnick, *Prog. Low Temp. Phys.*, C. J. Gorter, ed., (North-Holland, Amsterdam, 1970), Vol. 6, p. 37.
 - ⁷ C. Campbell, B. Clements, E. Krotschek, and M. Saarela, *Phys. Rev. B* **55**, 3769 (1997).
 - ⁸ J. Rutledge, W. McMillan, J. Mochel, and T. Washburn, *Phys. Rev. B* **18**, 2155 (1978).
 - ⁹ J. Nyecki, R. Ray, B. Cowan, and J. Saunders, *Phys. Rev. Lett.* **81**, 152 (1998).
 - ¹⁰ D. Bishop, J. Berthold, J. Parpia, and J. Reppy, *Phys. Rev. B* **24**, 5047 (1981).
 - ¹¹ S. Miyamoto and Y. Takano, *Czech. J. Phys.* **46**, suppl. S1, 137 (1996).
 - ¹² H. Cho and G. A. Williams, *Phys. Rev. Lett.* **75**, 1562 (1995).
 - ¹³ H. Cho and G. A. Williams, *J. Low Temp. Phys.* **101**, 463 (1995).
 - ¹⁴ H. Cho and G. A. Williams, *Czech. J. Phys.* **46**, suppl. S1, 47 (1996).
 - ¹⁵ H. Cho and G. A. Williams, *J. Low Temp. Phys.* **110**, 533 (1998).
 - ¹⁶ W. Saam and M. Cole, *Phys. Rev. B* **11**, 1086 (1975).
 - ¹⁷ M. Bernard and G. A. Williams, *Phys. Rev. Lett.* **67**, 2585 (1992).
 - ¹⁸ N. Mulders, J. Beamish, *Physica B* **165 & 166** 573 (1990).
 - ¹⁹ H. Chu and G. A. Williams, *Physica B* **284-288**, 335 (2000).
 - ²⁰ T. Minoguchi and Y. Nagaoka, *Prog. Theor. Phys.* **80**, 397 (1988); J. Machta and R. Guyer, *Phys. Rev. Lett.* **60**, 2054 (1988); F. Gallet and G. A. Williams, *Phys. Rev. B* **39**, 4673 (1989); G. A. Williams, *J. Low Temp. Phys.* **110**, 567 (1998).
 - ²¹ D. McQueeney, Ph.D. thesis, Cornell University, 1988, (unpublished).
 - ²² D. McQueeney, G. Agnolet, and J. Reppy, *Phys. Rev. Lett.* **52**, 1325 (1984).
 - ²³ R. Rosenbaum G.A. Williams, D. Heckerman, J. Marcus, D. Scholler, J. Maynard, and I. Rudnick, *J. Low Temp. Phys.* **37**, 663 (1979).
 - ²⁴ R. Hallock, in *Prog. Low Temp. Phys.*, W. Halperin, ed., (North-Holland, Amsterdam, 1996), Vol. 14, p. 321.